Sensors and Actuators B 197 (2014) 116–122

Contents lists available at ScienceDirect

Sensors and Actuators B: Chemical

journal homepage: www.elsevier.com/locate/snb

Colorimetric sensor arrays: Interplay of geometry, substrate and immobilization

Maria K. LaGasse[1], Jacqueline M. Rankin[1], Jon R. Askim, Kenneth S. Suslick*

Department of Chemistry, University of Illinois at Urbana-Champaign, 600 South Mathews Avenue, Urbana, IL 61801, United States

ARTICLE INFO

Article history:
Received 10 December 2013
Received in revised form 22 January 2014
Accepted 29 January 2014
Available online 19 February 2014

Keywords:
Colorimetric sensor array
Sensor optimization
Ormosil

ABSTRACT

This study addresses the interplay of geometry, substrate, and dye immobilization method on colorimetric sensor array performance. Arrays of cross-responsive dyes were exposed to either ammonia or sulfur dioxide gas at their permissible exposure levels (PEL) or their immediately dangerous to life or health (IDLH) concentrations and their colorimetric responses analyzed. Two-dimensional and linear arrays in flow cells were compared for flow path uniformity. Substrate effects were explored using arrays of 36 dyes immobilized in organically modified silica sol–gel (ormosil) formulations printed on six common substrates in three classes: impermeable (glass slides and polyethylene terephthalate), cellulose based (printer paper and chromatography paper with silica gel), and porous polymer membranes (polypropylene and polyvinylidene difluoride). The effect of immobilization of dyes in an ormosil versus in a plasticizer (i.e., a viscous semi-liquid) was also compared. The linear geometry showed a more homogeneous flow path than obtained with the two-dimensional array, which contributes to higher overall response, faster response, and better reproducibility. Arrays printed on impermeable substrates showed long response times attributed to slow diffusion of the analyte through the spot, and those printed on cellulose based substrates showed high noise caused by macroscale surface texturing. Arrays printed on porous polymer substrates showed the best spot quality and reproducibility, fastest response, and lowest noise. Finally, plasticizer and ormosils proved to be comparable immobilization matrices for colorants, and the preferred choice depends on the combination of dye, immobilization method, and substrate.

1. Introduction

The effectiveness of a colorimetric sensor array is influenced by not only the choice of chemoresponsive dyes, but also the choice of solid support, flow path geometry, and immobilization method [1–3]. These secondary factors can have a profound impact on the sensor's selectivity, sensitivity, dynamic range, response time, and thermal- and photo-stability [4–8]. While there are many variations in formulations of colorimetric sensors reported, a comprehensive comparison among the choices of these parameters has not been available.

Colorimetric sensor arrays utilize cross-responsive, chemically responsive dyes to generate a composite, olfactory-like response unique to a given odorant that can be quantified by digital imaging [1,2,4,9–14]. The colors of such dyes are affected by a wide range of intermolecular interactions between analyte and dye, including Brönsted and Lewis acid–base, hydrogen bonding, dipolar, and π–π interactions. In contrast, other array technologies rely on the weakest and least specific interactions between sensor and analyte (i.e., van der Waals and physical absorptions) [1,2,15–17]. While colorimetric sensor arrays have proven a powerful approach toward detection and differentiation of chemically diverse analytes, one encounters the problem of optimizing the inclusion of a large number of chemically diverse dyes into the sensor array without compromising desired functionality. Therefore, understanding the interplay of factors such as solid support and immobilization method on sensor response is central to improvements in the field.

Available solid supports for colorimetric sensor arrays are abundant in number, nature, and structure. The necessary properties of a solid support include optical transparency or high reflectivity, homogeneous structure, and general chemical compatibility [3]. For vapor sensing, an accessible substrate microstructure and high surface area enhance analyte diffusion to and high loading of the chromophore; hydrophobicity of the substrate will also help to reduce the effects of ambient humidity [9,10,18,19]. Organic polymer supports, such as cellulose derivatives or polyvinylidene difluoride, have been common substrates for many recent optical sensors because they satisfy many of these criteria and are, in general, commercially available with several types of microstructures. Inorganic substrates, such as glass, fused silica, or silica gel, are also widely used; while they are dimensionally stable (resistant to

* Corresponding author. Tel.: +1 217 333 2794; fax: +1 217 244 3186.
E-mail addresses: ksuslick@uiuc.edu, ksuslick@illinois.edu (K.S. Suslick).
[1] Contributed equally to this work.

0925-4005/$ – see front matter © 2014 Elsevier B.V. All rights reserved.
http://dx.doi.org/10.1016/j.snb.2014.01.102

swelling) and chemically inert, they may also have limited surface area and porosity.

Dye immobilization can be used to protect colorants in humid environments, mediate the transfer of dyes onto a solid support, prevent leaching into the sample medium, enhance the modulation of the optical properties, and improve analyte diffusion to reaction centers [6,20,21]. Two common immobilization materials are organically modified silanes (ormosils) and semi-liquid films of plasticizers or polymers. Ormosils can be tailored through the appropriate choice of sol–gel precursors and provide matrices with a range of hydrophobicity, nanoporosity, and surface area [22–26]. Plasticizers and polymers serve to solubilize the dye, facilitate analyte access to the reactive chromophores where analyte-colorant interaction occurs, and can act as selective sorbents, enhancing analyte selectivity [27,28]. Semi-liquid formulations have a similar range of potential polarities as ormosil matrices, but lack hierarchical porosity and high surface area.

We have previously described colorimetric sensor arrays [1,9,10] that can successfully differentiate among volatile organic compounds [18], toxic industrial chemicals (TICs) [4,26,29], beverages [30–32], and bacteria [33]. We have successfully employed both impermeable films (e.g., polyethylene terephthalate, PET) and permeable membranes (e.g., polyvinylidene difluoride, PVDF) as substrates, and used ormosils, polymers and plasticizers for dye immobilization. In this work, we explore the effect of array geometry, substrate, and immobilization method on sensor response. The response homogeneity, time, and magnitude of a new one-dimensional (linear) array configuration are compared to that of the previously reported two-dimensional (6×6) array configuration [4]. Additionally, we have chosen to examine six substrate materials: two impermeable (i.e., glass slides and PET), two paper (i.e., printer paper and chromatography paper with large pore silica gel (SG81)), and two porous polymer membranes (i.e., polypropylene (PP) and PVDF). To explore the effect of immobilization methods on dye reactivity, we compare the response of eight dyes immobilized either in previously optimized ormosil or as optimized plasticizer formulations. We report here a semi-quantitative evaluation of the influence of these secondary factors on colorimetric sensor array response, quality, consistency, and sensitivity.

2. Experimental

2.1. Materials

All reagents were of analytical grade and used without any further purification. Certified, premixed gas tanks were obtained from Matheson Tri-Gas through S.J. Smith. Substrates used included pre-cleaned glass slides (Gold Seal; thickness: 0.93–1.05 mm, size: $3 \times 1''$), PET (McMaster-Carr; thickness: 0.004 ± 0.0004 in.), SG81 chromatography paper (Whatman), multi-use paper (GP Spectrum), PP membrane (Sterlitech Corporation; thickness: 130–170 μm, pore size: 0.22 μm) and PVDF membrane (VWR Scientific, Batavia, IL; thickness: 165 μm, pore size: 0.45 μm).

2.2. Formulation preparation

Sol–gel solutions were prepared according to previous methods [4,24,25]. Briefly, sol–gel formulations were prepared by acid-catalyzed hydrolysis of solutions containing commercially-available silane precursors and low concentrations of surfactant dissolved in low volatility solvents. The surfactant acts to reduce capillary stress and improve print quality and the low volatility solvents act as porogens on the nanometer scale. The plasticizer formulation was prepared by adding tetraethylene glycol (10 wt%) to 2-methoxyethanol and stirring overnight [18]. The sol–gel or tetraethylene glycol solutions were added to chemoresponsive indicators (Table A.1) and mixed thoroughly by shaking. If appropriate, 1 M solutions of *t*-butylammonium hydroxide (TBAH) or *p*-toluenesulfonic acid (TsOH) in water were added immediately before printing.

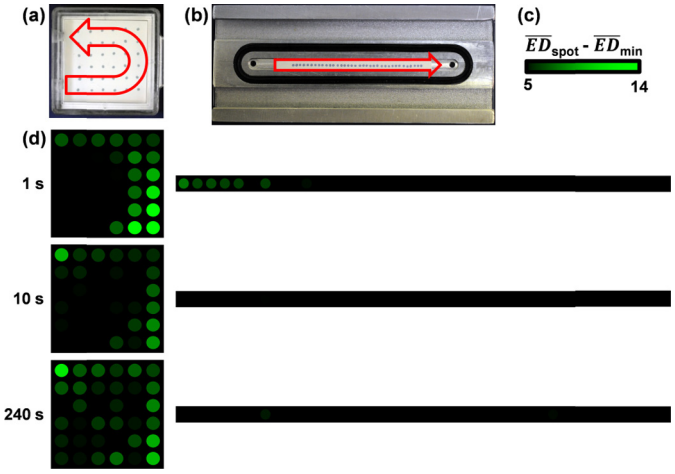

Fig. 1. Analysis of flow path for square vs. linear arrays. (a) Photograph of the 6×6 square array in cartridge showing the gas flow path. (b) Photograph of the linear array in holder showing the gas flow path. (c) Color coding of the spot to spot variation of sensor response (where $\overline{ED}_{spot}$ is the Euclidean distance from the ΔRGB values of each spot, and $\overline{ED}_{min}$ is the Euclidean distance of the sensor spot with the minimum change in color.) (d) Graphic depiction of gas flow inhomogeneity for 6×6 square vs. linear arrays at 1 s, 10 s, and 240 s upon exposure to NH_3 at PEL (50 ppm). (For interpretation of the references to color in this figure legend, the reader is referred to the web version of this article.)

2.3. Array printing

Formulations with chemoresponsive dyes were loaded into a Teflon ink well containing either a 6×6 or a 3×12 pattern of ~50 μL holes. An ArrayIt NanoPrint LM60 Microarray Printer (ArrayIt Corporation, Sunnyvale, CA) holding an array of floating slotted pins (delivering ~100 nL each) was used to robotically print arrays by dipping into the ink well and transferring to the substrate. For 6×6 arrays, all 36 spots were printed in one pass; linear arrays were printed in three passes, 12 at a time, in an interleaved linear pattern. Before use, ormosil arrays were stored in a nitrogen filled glove bag for three days and plasticizer arrays were stored first under vacuum at room temperature for 24 h and then in a nitrogen filled glove bag for two days.

2.4. Experimental procedure

Gas mixtures were prepared according to previous methods [4]. Briefly, MKS mass flow controllers were used to achieve gas streams with the desired concentration (50 ppm NH_3 or 100 ppm SO_2), flow (500 sccm) and relative humidity (50% RH) by mixing the appropriate amount of stock gas with wet (100% RH) and dry (0% RH) nitrogen gas. A MKS multigas analyzer (model 2030) was used in-line to verify gas concentrations. A diagram of the setup is shown in the supporting information (Fig. A.1). Arrays were exposed to a control stream (50% RH N_2) for 3 min followed by 4 min of an analyte stream. A Canon EOS 5D Mark II digital camera with a 100 mm macro lens was used to capture high definition video (30 fps) of the arrays lit with white LED strips ("natural white", SuperBrightLEDs.com).

6×6 arrays were contained within an injection molded disposable cartridge (dimensions of $22 \times 22 \times 4$ mm), as used in previous studies (Fig. 1a) [4,18,25]. Linear arrays were tested within flow

cells machined from Teflon or aluminum with channel dimensions of 1.6 × 0.5 × 57 mm and 3 × 0.6 × 57 mm, respectively (Fig. 1b). In both designs, an O-ring is placed in a groove around the channel and compressed by a glass slide to create a leak-free seal. Reflective substrates (PP, PVDF, SG81 and paper) were placed on the bottom of the aluminum holder channel and secured with silicone grease if necessary. Translucent substrates (glass slides and PET) were printed or secured to the glass slide and placed within the flow path of the Teflon holder.

To compare the linear and 6 × 6 array geometries, arrays of 36 identical spots of bromocresol green immobilized in an ormosil, were printed on PVDF in either a linear or 6 × 6 pattern. Arrays were exposed to NH_3 and run in quintuplicate. Substrate comparison was performed using arrays of 36 TICs responsive ormosil spots (Table A.1) printed on each substrate. Arrays were exposed to either NH_3 (all substrates) or SO_2 (PP and PVDF) and run in septuplicate. To compare dye immobilization materials, arrays of select dyes were printed using either ormosil or plasticizer formulations and exposed to NH_3 or SO_2 as described previously. These experiments were run in septuplicate.

2.5. Image processing and data analysis

GOM Media Player software was used to extract one still frame per second from video captured at 1920 × 1080 resolution (full HD). Images were processed using a customized software package, Spotfinder (iSense), which averaged the red, green and blue (*RGB*) values of an eight-pixel diameter area in the spot center. Δ*RGB* values were obtained by taking the difference of the *RGB* values from the before-exposure (i.e., after 3 min of nitrogen flow) and after-exposure images (i.e., after 4 min of analyte flow). This defines a 108-dimensional vector, i.e., 36 Δ*RGB* values, with each dimension ranging from −255 to +255 for eight-bit color imaging. The array response at a given timepoint is depicted pictorially using difference maps, an image generated from the Δ*RGB* absolute values for each spot in the array.

The Δ*RGB* values at a given timepoint can be combined into a Euclidean distance, defined by the equation $ED_t = (\Delta R_1^2 + \Delta G_1^2 + \Delta B_1^2 + \Delta R_2^2 + \cdots + \Delta B_n^2)_t^{1/2}$, where n is the number of spots under consideration and t is the time. To generate a response profile for a given analyte, the average Euclidean distance ($\overline{ED}$ for $n = 36$) at a given timepoint is plotted with respect to time. From this data, response time (defined here as the time necessary to reach 90% of the maximum *ED*) and relative standard deviation (RSD) is calculated. A map of the flow path at a given timepoint was generated by subtracting the $\overline{ED}$ value of the least responsive spot from the $\overline{ED}$ value of each spot in the array ($n = 1$). The ormosil and plasticizer formulations were compared using the equation: $\left(\overline{ED}_{\text{plasticizer}} - \overline{ED}_{\text{ormosil}}\right) / \left(\overline{ED}_{\text{plasticizer}} + \overline{ED}_{\text{ormosil}}\right)$.

2.6. Scanning electron microscopy

Scanning electron micrographs were obtained on a JEOL 7000F instrument operating at 15 kV with a medium probe current and a working distance of 10 mm. Samples were mounted to the holder via carbon tape and sputter coated with approximately 10 nm of Au/Pd prior to analysis to prevent surface charging.

3. Results and discussion

3.1. Geometry comparison

The flow path analysis of a 6 × 6 vs. a linear array holder is shown in Fig. 1. For the 6 × 6 array holder, the gas stream follows a U-shaped path traversing from the inlet, along the back wall, to the outlet. In contrast, a relatively homogeneous flow path is observed with the linear array holder. The inhomogeneous flow path in the 6 × 6 array holder contributes to a lower overall response, higher RSD, longer response time and less uniform array response (i.e., range of spot *ED* values) (Table 1). Spots in the 6 × 6 array that show the highest variation in color change are in locations where small differences in array position between trials brings the spot into or out of the analyte stream (Fig. A.2).

Table 1
Comparison of 6 × 6 and linear arrays exposed to ammonia at PEL (50 ppm).

	6 × 6	Linear
Average Euclidean distance (*ED*)[a] of 36 sensors	571	621
Relative standard deviation[a] (%)	3.1	0.79
Average time for 90% of total response after equilibration (s)	31	23
Range in *ED*[a,b] at 10 s	30.8	15.3

[a] From quintuplicate trials after 240 s analyte exposure.
[b] Maximum *ED* minus minimum *ED* among all sensors after 10 s exposure.

3.2. Substrate comparison

3.2.1. Spot quality

Spot quality was evaluated based on uniformity, size, and printing consistency. A qualitative ranking of the substrates, from highest to lowest, is PVDF ~ PP > PET > Glass > SG81 ~ Paper (Fig. 2).

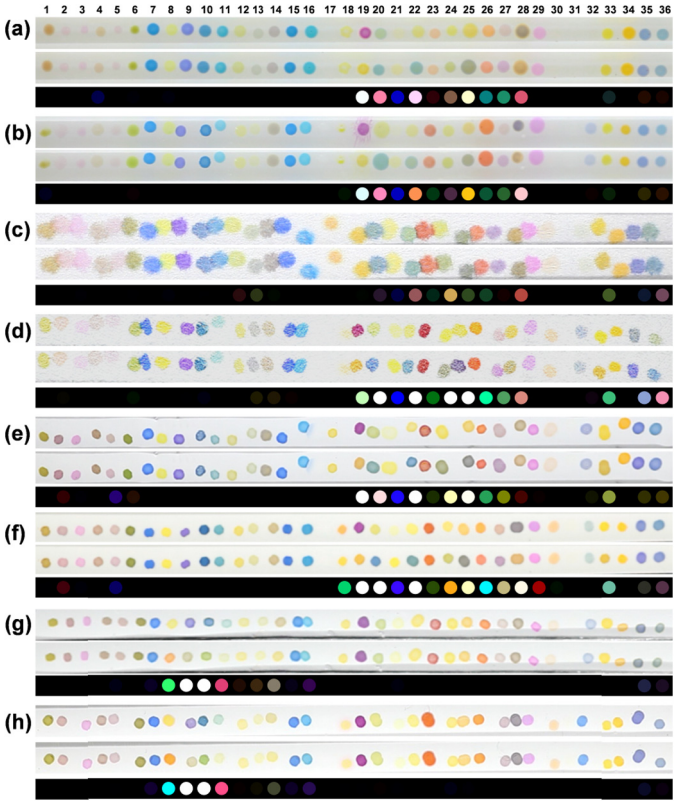

Fig. 2. Raw images and difference maps for arrays printed on various substrates exposed to (a–f) NH_3 (50 ppm) and (g and h) SO_2 (100 ppm). (a) Glass slide, (b) polyethylene terephthalate, (c) printer paper, (d) SG81 chromatography paper, (e) polypropylene membrane, (f) polyvinylidene difluoride membrane, (g) polypropylene membrane, (h) polyvinylidene difluoride membrane. For each substrate (a–h), the top image is the array before exposure, the middle image is after exposure, and the bottom is the difference map (red value minus red value, green minus green, blue minus blue). For display purposes, the color ranges of these difference maps are expanded from five to eight bits per color (*RGB* range of 2–33 expanded to 0–255). (For interpretation of the references to color in this figure legend, the reader is referred to the web version of this article.)

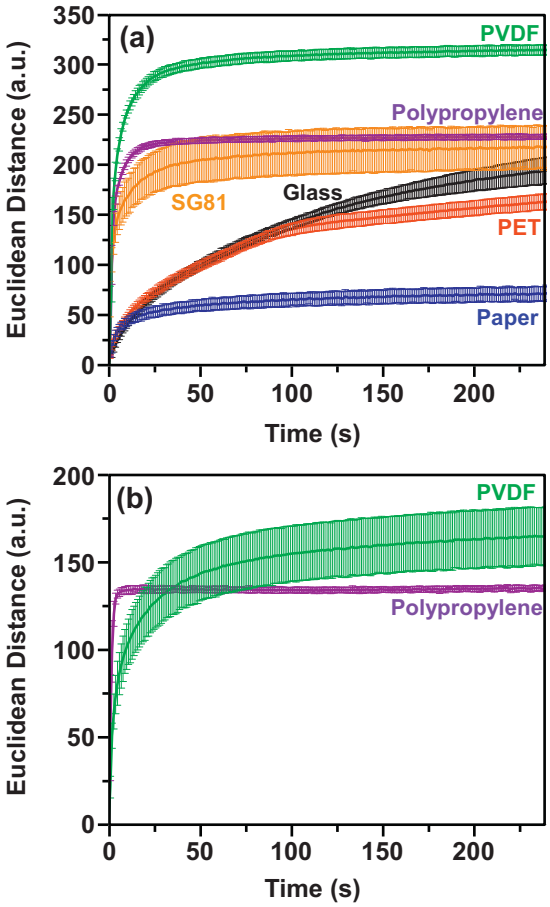

Fig. 3. Euclidean distance versus time graphs for ormosil arrays printed on various substrates exposed to (a) NH_3 (50 ppm) and (b) SO_2 (100 ppm).

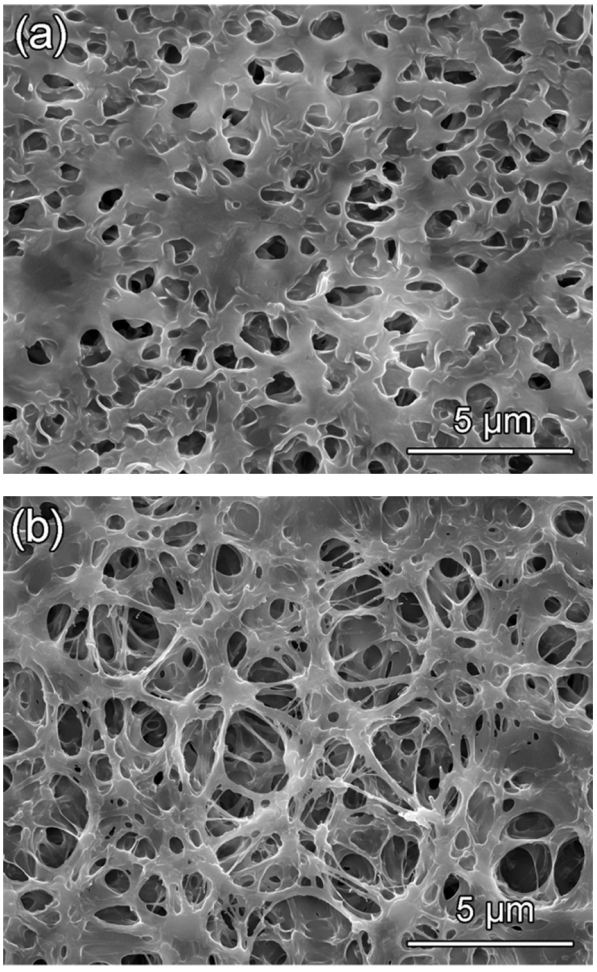

Fig. 4. Scanning electron micrographs of ormosil spots printed on (a) polyvinylidene difluoride (PVDF) and (b) polypropylene (PP) membranes.

Spots printed on PVDF were well formed, evenly colored and consistent among arrays in both color and size. The spots printed on PP were similar in quality but with a slightly more noticeable "coffee-ring effect". We speculate this may be mitigated by using a different surfactant, surfactant concentration, or solvent. Most spots printed on PET exhibited similar uniformity and consistency; however, some were very small (e.g., spot 18) or showed a spider-web effect (e.g., spot 19). The color and size of spots printed on glass were inconsistent.

The paper substrates produced the poorest quality arrays. Spots on both SG81 and paper were relatively uniform in size and color, but were inhomogeneous throughout, largely due to the macroscale surface texture of the papers themselves combined with significant spreading due to capillary action. This was especially problematic for spots printed on printer paper and uncoated chromatography paper (not shown), where the spots were so large that they abutted or overlapped adjacent spots.

3.2.2. Array response

A comparison of arrays printed with ormosil immobilized dyes on each substrate is given in Table 2 for response to NH_3 at 50 ppm (PEL) and SO_2 at 100 ppm (IDLH). The total *ED* with respect to time for the arrays upon exposure to NH_3 and SO_2 are given in Fig. 3.

Upon exposure to NH_3 or SO_2, arrays printed on PVDF showed a significantly higher total response than those printed on other substrates. There were spot dependent changes in signal observed that correlate to differences in initial spot color among substrates (Fig. 2); this may be reflective of variations in the acid/base properties and chemical functionality of each substrate. We suggest this could largely be overcome by optimizing the dye formulations for each substrate (e.g., through the addition of small amounts of acid or base before printing). The decrease in signal for the PET and glass slide arrays is dominated by the larger distance between the array and the reflective white background (i.e., the Teflon holder), which could be ameliorated by increasing the illumination.

Upon exposure to NH_3, arrays printed on impermeable substrates (glass and PET) showed a slower response time relative to the porous substrates (Paper, SG81, PP and PVDF), which we attribute to slower diffusion of the analyte through the ormosil matrix caused by reduced hierarchical porosity. The RSD, a major limiting factor in the arrays' potential for discriminating among analytes, was significantly lower for arrays printed on porous polymer substrates: e.g., the NH_3 responsive spots printed on PP and PVDF were more consistent between printings of arrays than those printed on other substrates. Arrays printed on the paper substrates showed significantly higher noise due to inhomogeneity within the spots as discussed in Section 3.2.1.

When exposed to SO_2, arrays printed on PP and PVDF membranes had very different response profiles (Table 2 and Fig. 3b). Arrays on PP were two to three times faster to respond than arrays on PVDF for both NH_3 and SO_2. The faster reaction times for sensors on PP correlates with the SEM images of spots printed on PVDF and PP (Fig. 4) that show increased porosity and surface area for the dye-coated PP versus PVDF. In addition, PVDF arrays had higher RSD (and thus poorer reproducibility) than PP arrays, which suggests

Table 2
Comparison of analyte response of arrays printed on various substrates.

	NH_3 (50 ppm)						SO_2 (100 ppm)	
	Glass	PET	Paper	SG81	PP	PVDF	PP	PVDF
Average Euclidean distance[a]	199.7	163.2	72.0	218.1	228.0	314.6	135.7	165.3
Relative standard deviation[a] (%)	8.0	4.8	11.4	4.4	1.1	1.5	1.2	9.9
Response time (s)	173	143	91	31	12	23	4	68
Noise[b]	0.655	0.614	0.898	0.920	0.591	0.555	0.546	0.646

[a] Septuplicate trials after 240 s analyte exposure.
[b] Standard deviation of the residuals from a linear regression of the control response for all non-saturated channels over all trials.

Table 3
Average Euclidean distances and standard deviations for dyes immobilized in plasticizers or ormosils. The most responsive formulation/substrate combination for each dye is shown in boldface.

	Polypropylene		PVDF	
	Plasticizer	Ormosil	Plasticizer	Ormosil
Methyl red + TBAH	65.9 ± 1.6	42.0 ± 3.1	51.2 ± 2.1	**70.5 ± 4.8**
Chlorophenol red + TBAH	**128.2 ± 4.1**	69.2 ± 3.9	54.3 ± 1.7	73.7 ± 6.6
Nitrazine yellow + TBAH	**163.2 ± 6.4**	93.1 ± 2.3	56.3 ± 2.6	114.2 ± 4.8
Bromothymol blue + TBAH	**185.4 ± 4.1**	35.1 ± 2.9	133.8 ± 4.3	44.6 ± 8.7
Fluorescein	56.0 ± 1.4	60.5 ± 3.3	29.4 ± 1.6	**93.6 ± 5.6**
Bromocresol green	185.1 ± 3.6	114.2 ± 3.2	**197.0 ± 8.1**	132.7 ± 3.0
Bromophenol red	**136.7 ± 3.5**	89.6 ± 2.0	77.2 ± 2.8	108.4 ± 3.0
Nile red	1.6 ± 0.3	3.0 ± 0.8	10.7 ± 1.9	**21.2 ± 1.7**

the printing consistency of the SO_2 responsive spots was worse on PVDF.

3.3. Formulation comparison

Fig. 5 shows a comparison of the relative responses of each plasticizer and ormosil spot printed on PP and PVDF membranes upon exposure to NH_3 or SO_2. In general, the plasticizer formulations were favored on PP, whereas the ormosil formulations were favored on PVDF. There were exceptions, however, and the most responsive dye/formulation combination was dependent on both dye identity and substrate (Table 3). When printed on PP, the SO_2 sensitive spots showed a universal increase in response when immobilized in a plasticizer versus ormosil matrix. This trend was not observed with the spots printed on PVDF, and all but bromothymol blue + TBAH showed a higher response when immobilized in ormosils. The higher signal for the plasticizer immobilized dyes was likely due to improved spot uniformity and color intensity (Fig. 6), apparent in the before and after images of the bromothymol blue + TBAH on both PP and PVDF. Spot response was not solely dependent on dye concentration, as many of the plasticizer spots were more sensitive despite a lower dye concentration (e.g., methyl red + TBAH). The nile red and fluorescein dyes (NH_3 sensitive) showed a much higher response when immobilized in

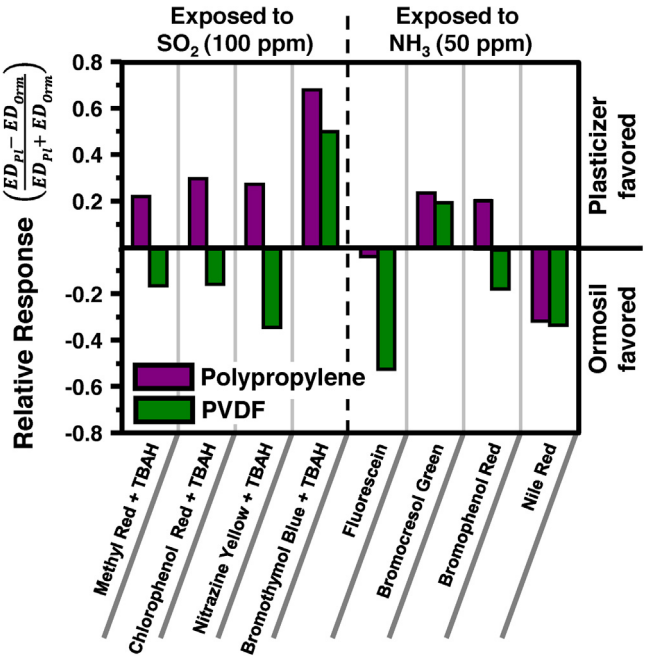

Fig. 5. Comparison of plasticizer and ormosil immobilized colorants printed on polypropylene and polyvinylidene difluoride (PVDF) and exposed to SO_2 (100 ppm) or NH_3 (50 ppm).

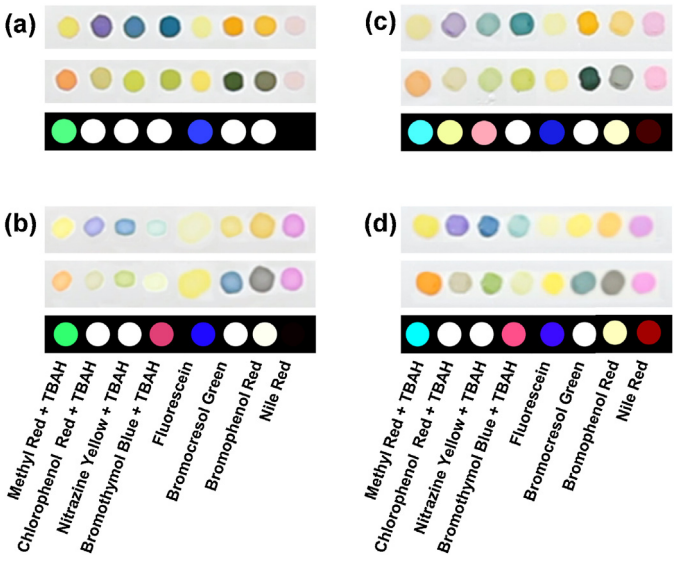

Fig. 6. Raw images and difference maps for arrays of plasticizer (a and c) and ormosil (b and d) immobilized colorants printed on polypropylene (a and b) or polyvinylidene difluoride (c and d) membranes upon exposure to SO_2 (100 ppm) or NH_3 (50 ppm). Within the images for each formulation: (top) image of array before exposure, (middle) image of array after exposure, and (bottom) difference map. For display purposes, the color ranges of these difference maps are expanded from five to eight bits per color (RGB range of 2-33). (For interpretation of the references to color in this figure legend, the reader is referred to the web version of this article.)

ormosils versus plasticizer, and the before images showed a discrepancy in the starting color of these dyes when immobilized in plasticizer versus ormosil. We speculate this may be due to non-optimal spot pH or differences in matrix polarity. Array-to-array reproducibility was similar between ormosil and plasticizer immobilized dyes (Table 3).

4. Conclusions

This work has demonstrated the importance and interdependence of geometry, substrate, and immobilization method on colorimetric sensor array response. Linearization of the array provides many benefits, including a more uniform response, a higher overall signal, a shorter response time, and better reproducibility. Additionally, a linear array has greater experimental versatility than a two-dimensional array: e.g., linear arrays are suitable for kinetic measurements and may be imaged with one-dimensional (line) scanners with much higher scan rates. Arrays printed in ormosil formulations on impermeable substrates have longer response times than those printed on permeable substrates, likely caused by a lack of hierarchical porosity and limited analyte diffusion through the sensor spot. The difference in response time of the less-porous PVDF arrays and the more-porous PP arrays provides further evidence of the importance of substrate porosity in sensor response time. Cellulose substrates have intermediate response times, but also have higher noise due to their highly textured surface. Arrays printed on porous polymer membranes exhibited the fastest reaction times, the best reproducibility, and the lowest noise. The optimum immobilization matrix is highly dependent on dye identity, formulation, and substrate. In general, plasticizer formulations were preferred for PP while ormosil formulations were preferred for PVDF.

Acknowledgments

This work was carried out in part in the Frederick Seitz Materials Research Laboratory Central Facilities, University of Illinois. This work was supported by the Dept. of Defense (JIEDDO/TSWG CB3614), the National Science Foundation Graduate Research Fellowship Program under Grant no. DGE-1144245 (JMK), and a Department of Education GAANN Fellowship (MKL). JMR gratefully acknowledges fellowship support from the Rober C. and Carolyn J. Springborn Endowment. We greatly appreciate the machining assistance of the School of Chemical Sciences Machine Shop, University of Illinois at Urbana-Champaign.

Appendix A. Supplementary data

Supplementary data associated with this article can be found, in the online version, at http://dx.doi.org/10.1016/j.snb.2014.01.102.

References

[1] J.R. Askim, M. Mahmoudi, K.S. Suslick, Optical sensor arrays for chemical sensing: the optoelectronic nose, Chem. Soc. Rev. 42 (2013) 8649–8682.
[2] K.L. Diehl, E.V. Anslyn, Array sensing using optical methods for detection of chemical and biological hazards, Chem. Soc. Rev. 42 (2013) 8596–8611.
[3] O. Guillermo, M. Moreno-Bondi, D. Garcia-Fresnadillo, M. Marazuela, The interplay of indicator, support and analyte in optical sensor layers, in: G. Orellana, M. Moreno-Bondi (Eds.), Frontiers in Chemical Sensors, Springer, Berlin, Heidelberg, 2005, pp. 189–225.
[4] S.H. Lim, L. Feng, J.W. Kemling, C.J. Musto, K.S. Suslick, An optoelectronic nose for the detection of toxic gases, Nat. Chem. 1 (2009) 562–567.
[5] Z. Zhu, L. Garcia-Gancedo, A.J. Flewitt, H. Xie, F. Moussy, W.I. Milne, A critical review of glucose biosensors based on carbon nanomaterials: carbon nanotubes and graphene, Sensors 12 (2012) 5996–6022.
[6] P.C.A. Jeronimo, A.N. Araujo, M.C.B.S.M. Montenegro, Optical sensors and biosensors based on sol–gel films, Talanta 72 (2007) 13–27.
[7] C. Rottman, G. Grader, Y. De Hazan, S. Melchior, D. Avnir, Surfactant-induced modification of dopants reactivity in sol–gel matrixes, J. Am. Chem. Soc. 121 (1999) 8533–8543.
[8] J.M. Costa-Fernández, A. Sanz-Medel, Air moisture sensing materials based on the room temperature phosphorescence quenching of immobilized mercurochrome, Anal. Chim. Acta 407 (2000) 61–69.
[9] K.S. Suslick, D.P. Bailey, C.K. Ingison, M. Janzen, M.E. Kosal, W.B. McNamara III, et al., Seeing smells: development of an optoelectronic nose, Quim. Nova 30 (2007) 677–681.
[10] K.S. Suslick, N.A. Rakow, A. Sen, Colorimetric sensor arrays for molecular recognition, Tetrahedron 60 (2004) 11133–11138.
[11] N.A. Rakow, K.S. Suslick, A colorimetric sensor array for odour visualization, Nature 406 (2000) 710–713.
[12] K.S. Suslick, An optoelectronic nose:"seeing" smells by means of colorimetric sensor arrays, MRS Bull. 29 (2004) 720–725.
[13] Y. Salinas, J.V. Ros-Lis, J.-L. Vivancos, R. Martínez-Máñez, S. Aucejo, N. Herranz, et al., A chromogenic sensor array for boiled marinated turkey freshness monitoring, Sens. Actuators, B 190 (2014) 326–333.
[14] T. Soga, Y. Jimbo, K. Suzuki, D. Citterio, Inkjet-printed paper-based colorimetric sensor array for the discrimination of volatile primary amines, Anal. Chem. 85 (2013) 8973–8978.
[15] L. Torsi, M. Magliulo, K. Manoli, G. Palazzo, Organic field-effect transistor sensors: a tutorial review, Chem. Soc. Rev. 42 (2013) 8612–8628.
[16] A. Grinthal, J. Aizenberg, Adaptive all the way down: building responsive materials from hierarchies of chemomechanical feedback, Chem. Soc. Rev. 42 (2013) 7072–7085.
[17] J. Tamayo, P.M. Kosaka, J.J. Ruz, A. San Paulo, M. Calleja, Biosensors based on nanomechanical systems, Chem. Soc. Rev. 42 (2013) 1287–1311.
[18] M.C. Janzen, J.B. Ponder, D.P. Bailey, C.K. Ingison, K.S. Suslick, Colorimetric sensor arrays for volatile organic compounds, Anal. Chem. 78 (2006) 3591–3600.
[19] J.W. Kemling, A.J. Qavi, R.C. Bailey, K.S. Suslick, Nanostructured substrates for optical sensing, J. Phys. Chem. Lett. 2 (2011) 2934–2944.
[20] B.D. MacCraith, C.M. McDonagh, G. O'Keeffe, A.K. McEvoy, T. Butler, F.R. Sheridan, Sol–gel coatings for optical chemical sensors and biosensors, Sens. Actuators, B 29 (1995) 51–57.
[21] I.M. Steinberg, A. Lobnik, O.S. Wolfbeis, Characterisation of an optical sensor membrane based on the metal ion indicator Pyrocatechol Violet, Sens. Actuators, B 90 (2003) 230–235.
[22] A. Lukowiak, S. Wieslaw, Sensing abilities of materials prepared by sol–gel technology, J. Sol–Gel Sci. Technol. 50 (2009) 201–215.
[23] H. Podbielska, Ulatowska-Jarka, G. Muller, H.J. Eichler, Sol–Gels for Optical Sensors, Springer, Erice, Italy, 2006.
[24] J.W. Kemling, K.S. Suslick, Nanoscale porosity in pigments for chemical sensing, Nanoscale 3 (2011) 1971–1973.
[25] S.H. Lim, J.W. Kemling, L. Feng, K.S. Suslick, A colorimetric sensor array of porous pigments, Analyst 134 (2009) 2453–2457.
[26] L. Feng, C.J. Musto, J.W. Kemling, S.H. Lim, K.S. Suslick, A colorimetric sensor array for identification of toxic gases below permissible exposure limits, Chem. Commun. 46 (2010) 2037–2039.
[27] I. Levitsky, S.G. Krivoshlykov, J.W. Grate, Rational design of a Nile Red/polymer composite film for fluorescence sensing of organophosphonate vapors using hydrogen bond acidic polymers, Anal. Chem. 73 (2001) 3441–3448.
[28] R.D. Johnson, L. Bachas, Ionophore-based ion-selective potentiometric and optical sensors, Anal. Bioanal. Chem. 376 (2003) 328–341.
[29] L. Feng, C.J. Musto, J.W. Kemling, S.H. Lim, W. Zhong, K.S. Suslick, Colorimetric sensor array for determination and identification of toxic industrial chemicals, Anal. Chem. 82 (2010) 9433–9440.
[30] B.A. Suslick, L. Feng, K.S. Suslick, Discrimination of complex mixtures by a colorimetric sensor array: coffee aromas, Anal. Chem. 82 (2010) 2067–2073.
[31] C. Zhang, D.P. Bailey, K.S. Suslick, Colorimetric sensor arrays for the analysis of beers: a feasibility study, J. Agric. Food Chem. 54 (2006) 4925–4931.
[32] C. Zhang, K.S. Suslick, Colorimetric sensor array for soft drink analysis, J. Agric. Food Chem. 55 (2007) 237–242.
[33] J.R. Carey, K.S. Suslick, K.I. Hulkower, J.A. Imlay, K.R.C. Imlay, C.K. Ingison, et al., Rapid identification of bacteria with a disposable colorimetric sensing array, J. Am. Chem. Soc. 133 (2011) 7571–7576.

Biographies

Maria K. LaGasse received her B.S. in chemistry and physical science in 2010 from St. John's University in Queens, NY. She is currently working on her Ph.D. in inorganic chemistry from the University of Illinois at Urbana-Champaign. Her research interests include the development, optimization, and application of chemical sensors and understanding the systems in which they operate.

Jacqueline M. Rankin is pursuing her Ph.D. in inorganic chemistry at the University of Illinois at Urbana-Champaign. She is a recipient of both the National Science Foundation Graduate Research Fellowship and UIUC's Springborn Fellowship. Her research interests include colorimetric sensing, disposable and portable sensing technology, and micro gas chromatography. She received her B.S. in chemistry and B.S. in secondary education from Kansas State University in 2011.

Jon R. Askim grew up in Vancouver, WA, and received his B.S. in Chemistry from Western Washington University. He is currently completing his Ph.D. in the

Department of Chemistry of the University of Illinois at Urbana-Champaign in the Suslick Research Group.

Kenneth S. Suslick is the Marvin T. Schmidt Professor of Chemistry, a professor of materials science and engineering, and a Beckman Institute Professor at the University of Illinois at Urbana-Champaign. Professor Suslick received his B.S. from Caltech in 1974, Ph.D. from Stanford in 1978, and joined UIUC immediately thereafter. Suslick has published more than 325 papers, edited four books, and holds 25 patents. His research expertise includes chemical sensing, catalytic and functional nano-materials, metalloporphyrins and bioinorganic chemistry, and the physical and chemical effects of ultrasound. Suslick is the recipient of the Sir George Stokes Medal of the RSC, the ACS Nobel Laureate Signature Award for Graduate Education, the MRS Medal, the ACS Senior Cope Scholar Award, the ASA Mentorship Award, a Guggenheim Fellowship, and the Silver Medal of the Royal Society for Arts, Manufactures and Commerce. He is a Fellow of the AAAS, the ACS, the MRS, the RSC, and the ASA.